

# Electron Transport Limitation in P3HT:CdSe Nanorods Hybrid Solar Cells

Jun Yan Lek,<sup>†,#</sup> Guichuan Xing,<sup>‡,§,#</sup> Tze Chien Sum,<sup>\*,‡,§,||</sup> and Yeng Ming Lam<sup>\*,†,||,⊥</sup>

<sup>†</sup>School of Materials Science and Engineering, Nanyang Technological University, 50 Nanyang Avenue, Singapore 639798

<sup>‡</sup>School of Physical and Mathematical Sciences, Nanyang Technological University, 21 Nanyang Link, Singapore 637371

<sup>§</sup>Singapore-Berkeley Research Initiative for Sustainable Energy (SinBeRISE), 1 Create Way, Singapore 138602

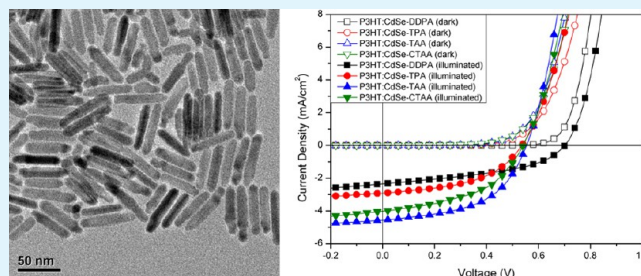
<sup>||</sup>Energy Research Institute @ NTU (ERI@N), Nanyang Technological University, 50 Nanyang Drive, Singapore 637533

<sup>⊥</sup>Institute of Materials for Electronic Engineering II, RWTH-Aachen, Sommerfeldstraße 24, D-52074 Aachen, Germany

## Supporting Information

**ABSTRACT:** Hybrid solar cells have the potential to be efficient solar-energy-harvesting devices that can combine the benefits of solution-processable organic materials and the extended absorption offered by inorganic materials. In this work, an understanding of the factors limiting the performance of hybrid solar cells is explored. Through photovoltaic-device characterization correlated with transient absorption spectroscopy measurements, it was found that the interfacial charge transfer between the organic (P3HT) and inorganic (CdSe nanorods) components is not the factor limiting the performance of these solar cells. The insulating original ligands retard the charge recombination between the charge-transfer states across the CdSe–P3HT interface, and this is actually beneficial for charge collection. These cells are, in fact, limited by the subsequent electron collection via CdSe nanoparticles to the electrodes. Hence, the design of a more continuous electron-transport pathway should greatly improve the performance of hybrid solar cells in the future.

**KEYWORDS:** hybrid solar cells, ligand exchange, transient absorption, charge transport



## INTRODUCTION

In recent years, organic and hybrid solar cells have been considered as possible cost-effective solutions for energy harvesting and conversion. These cells are generally lightweight, relatively thin, strongly light-absorbing, and solution-processable, making this technology very attractive for the large-scale fabrication of flexible solar cells. Organic–inorganic hybrid solar cells (HSCs) essentially consist of both organic molecules/polymers and inorganic semiconducting nanocrystals as electron donors or acceptors in the photoactive layer. Inorganic nanocrystals offer several attractive properties such as a tunable band gap, a higher intrinsic charge mobility, the possibility of multiple exciton generation if the band gap is sufficiently small, and so forth. Some of the inorganic nanocrystals typically used for the fabrication of HSCs include cadmium chalcogenides, lead(II) chalcogenides, titania (TiO<sub>2</sub>), zinc oxide (ZnO), and others.<sup>1–15</sup> To date, cadmium selenide (CdSe) nanocrystals are the most widely investigated acceptors in HSCs because they are readily synthesized into a wide variety of shapes and sizes with solution-based synthetic routes.<sup>1–3,16–20</sup>

The syntheses of inorganic nanocrystals are often carried out in the presence of organic surfactants or ligands such as trioctylphosphine oxide (TOPO), phosphonic acids, fatty acids,

fatty amines, and so forth.<sup>19,21–24</sup> These ligands have several functions, such as passivation of the nanocrystals surface, providing colloidal stability and directing the growth of the nanocrystals.<sup>25</sup> They are usually bulky and electrically insulating and therefore hinder charge transfer and transport when the nanocrystals are fabricated into electronic devices. Post-synthesis surface modification, also known as ligand exchange, is often carried out to replace the original bulky organic surfactants using smaller molecules such as pyridine, amines, thiols, thiophene-based molecules, and so forth.<sup>1–3,26–32</sup> Since the pioneering work by Huynh et al., pyridine has been the most widely studied replacing ligand for CdSe nanocrystals in HSCs applications. HSCs made of pyridine-treated CdSe nanocrystals were reported to have better charge transport as a result of the reduced interparticle distance after ligand exchange.<sup>1</sup> The best HSCs device so far is based on CdSe-based HSCs fabricated using a mixture of pyridine-treated nanorods and quantum dots together with poly[2,1,3-benzothiadiazole-4,7-diyl[4,4-bis(2-ethylhexyl)-4H-cyclopenta[2,1-b:3,4-b']dithiophene-2,6-diyl]] (PCPDTBT) as donor,

**Received:** September 25, 2013

**Accepted:** December 18, 2013

**Published:** December 18, 2013

with a 3.6% power conversion efficiency (PCE).<sup>33</sup> One of the challenges in these systems is the necessity of a solvent mixture to aid the dispersion of pyridine-treated nanocrystals. In a previous work, we showed that with thiophene-amine molecules as the replacing ligand for CdSe nanorods, comparable hybrid film morphology and HSC performance to those made of pyridine-treated nanorods was achieved.<sup>32</sup>

Carboxylic acid-based molecules have also proven to be promising surface capping ligands for inorganic nanocrystals.<sup>12,13,26,34,35</sup> They have been widely used as ligands for metal-oxide nanocrystals, such as TiO<sub>2</sub>, because of the high binding energy between the carboxylic acid group and the metal-oxide surface. Lin et al. studied the ligand exchange of TiO<sub>2</sub> nanocrystals using several carboxylic acid-based molecules and have shown HSCs devices with a PCE of 2.2% using poly(3-hexylthiophene) (P3HT) and TiO<sub>2</sub> nanorods after ligand exchange with one such molecule: *cis*-bis(4,4-dicarboxy-2,2-bipyridine)dithiocyanato ruthenium(II) (N3-dye).<sup>13</sup> However, in work by Bouclé et al., charge-separation efficiency increased but charge-transport efficiency remained poor after ligand exchange of TOPO with ruthenium dye (*cis*-bis-(isothiocyanato)(2,2'-bipyridyl-4,4'-dicarboxylato)(2,2'-bipyridyl-4'-dinonyl)ruthenium) (Z907).<sup>36</sup> Unlike metal-oxide nanocrystals, there are very few studies on the ligand exchange of metal chalcogenide nanocrystals with carboxylic acids or its derivatives. This is probably due to the lower binding energy of carboxylic acids as compared to phosphonic acids and amines on the metal chalcogenide surfaces.<sup>37</sup> Cadmium sulfide (CdS) nanorods have been modified using carboxylic acid-based molecules.<sup>35</sup> A 10-fold increase in PCE after modification with anthracene-9-carboxylic acid (ACA) was observed because of a reduction in the surface traps and improved compatibility between the P3HT and the nanorods. Olson et al. have also demonstrated the ligand exchange of CdSe nanocrystals with various ligands including carboxylic acids; however, the photovoltaic properties were not shown in that report.<sup>26</sup> It was observed that HSCs made with oleic acid-treated and stearic acid-treated CdSe nanocrystals did not perform as well as those prepared using butylamine-treated nanocrystals because of the higher resistance arising from the insulating alkyl chain of the two acids. Although devices fabricated using nanocrystals with carboxylic acid-based ligands do not perform as well as their amine counterparts, these ligands offer a greener option as compared to phosphorus-based ligands. Furthermore, carboxylic acids are also found to have greater selectivity compared to amines for different CdSe and CdS nanocrystals facets. Such selectivity is essential in the controlled synthesis of one-dimensional (1D) nanocrystals.<sup>37,38</sup> Amines have strong affinity for the (11 $\bar{2}$ 0), (000 $\bar{1}$ ), and (0001) facets in contrast to the moderate affinity to these facets for carboxylic acids, but the latter is highly selective of the (11 $\bar{2}$ 0) facet.<sup>38</sup> Because of this selectivity, carboxylic acid-based molecules are highly suitable for the in situ synthesis of 1D CdSe nanocrystals and thus offer the possibility to eliminate the postsynthesis surface-modification step.

As mentioned, in hybrid devices, organic ligands are necessary because these molecules control the synthesis and the dispersion of the nanocrystals in both solution and thin films. Hence, it is very important to understand the implications of these surface capping ligands on the charge transfer at the donor/acceptor interface and charge transport between the nanocrystals. The charge-transfer dynamics between donor and acceptor in various heterojunction systems can be investigated

using transient absorption spectroscopy (TAS).<sup>39–43</sup> It was found that the yield of the photogenerated charges is strongly influenced by the crystallinity of the inorganic phase in organic–inorganic hybrid systems.<sup>44</sup> In addition, it was also found from TAS that the electron-transfer rate and the process are affected by the amount of donor–acceptor interfaces and their location along the nanocrystals (enhanced at the tips).<sup>40,42</sup> It was shown that the mercaptocarboxylic acid ligands on the CdSe nanocrystals have a strong influence on the electron-transfer rate between CdSe and polymeric viologen and that the electron-transfer rate increased with decreasing ligand length.<sup>45</sup> However, it was also reported that the electron transfer depends on the conformation of the ligands attached onto the nanocrystals. Morris-Cohen et al. reported that the electron-transfer rate was independent of the alkyl chain length when the prominent transfer pathway was not along the molecular axis of viologen derivatives.<sup>46</sup> In general, it is believed that ligands prevent efficient charge transfer between the nanocrystals and the polymer and also efficient charge transport between the nanocrystals.<sup>2,16</sup>

Hence, in view of the potential use of these carboxylic acid-based molecules as both the ligands for controlled synthesis and also as interface-modifying ligands for improving the device performance, the effect of these molecules as replacing ligands on the HSCs performance is explored in this work. Several carboxylic acid-based molecules were exchanged for the original growth control ligand, dodecylphosphonic acid (DDPA): 2-thiophenepropionic acid (TPA), 2-thiopheneacrylic acid (TAA), and 2-cyano-3-(thiophen-2-yl) acrylic acid (CTAA). These replacing ligands were selected on the basis of several considerations: (a) small molecules are preferred, (b) affinity for CdSe surfaces, and (c) compatibility with polymer donor. To elucidate the factors that limit the performance of hybrid solar cells, transient absorption spectra of the HSCs made with different ligand-treated CdSe nanorods were collected. On the basis of the lifetime measurements, it was found that the ligands do not limit hole transfer across the CdSe–P3HT interface. In fact, with more insulating ligands, the charge recombination between the charge-transfer states across the CdSe–P3HT interface is retarded, which is beneficial for charge collection. The issue with these systems is the subsequent charge transport between the nanocrystals as the electrons move toward the electrode, which is limited by the conductivity between the neighboring nanocrystals.

## ■ EXPERIMENTAL SECTION

**Materials.** Trioctylphosphine (TOP, 90%) and cadmium oxide (CdO, 99.95%) were purchased from Fluka. Dodecylphosphonic acid (DDPA, 100%) was obtained from Polycarbon Inc. TOPO (99%) and selenium powders (Se, 99%) were purchased from Sigma-Aldrich and Kanto Chemical, respectively. P3HT (grade 4002-EE) with 90–93% regioregularity and molecular weight ranges from 48 000 g/mol was purchased from Rieke Metal Inc. Poly(3,4-ethylenedioxythiophene)-poly(styrenesulfonate) (PEDOT:PSS, CLEVIOS AL 4083) was obtained from H.C. Stark. 1,2-Dichlorobenzene (DCB, CHROMASOLV 99%), acetone (>99.5%), pyridine (>99.0%), and methanol (anhydrous, 99.8%) were purchased from Sigma-Aldrich. Toluene (extra dry) was obtained from Acros Organics. TPA (98%) was obtained from Sigma-Aldrich. TAA (>98%) was purchased from Alfa Aesar. CTAA was synthesized with the help from Dr. Hairong Li using a modified route from ref 47. All of the chemicals were used without further purification.

**Synthesis of CdSe Nanorods.** CdSe nanorods were synthesized using hot coordinating solvents method.<sup>20</sup> In a typical CdSe nanoparticles synthesis, 256 mg (2 mmol) of CdO, 1.0 g (4 mmol)

of DDPA, and 2.5 g of TOPO were loaded into a three-necked flask equipped with a condenser and thermometer. The mixture was then heated at 330 °C. The solution mixture turned colorless, indicating the formation of Cd–DDPA complexes at elevated temperature. The solution was then cooled to 310 °C and held at constant temperature. Selenium precursor solution consisting of 156 mg (2 mmol) of selenium powder and 2.0 g of TOP was injected into the cadmium precursor solution using a multiple-injections method (four times at 2 min intervals). The nanocrystals were allowed to grow for 30 min. The reaction was stopped by removing the reaction flask from the heating mantle. CdSe nanorods were dispersed in anhydrous toluene and precipitated with anhydrous methanol. The solution was then centrifuged, and the nanorods were collected. This process was repeated several times to remove the free ligands, and eventually the nanorods were redispersed in toluene for further characterization, surface modification, and device fabrication. The as-synthesized CdSe nanorods will be identified as CdSe–DDPA in the following text.

**Ligand Exchange.** For ligand exchange using TPA, 100 mg of CdSe nanorods and 625 mg (4 mmol) of TPA were first dispersed in 7 and 3 mL of toluene separately. After both CdSe nanorods and TPA were dispersed and dissolved, the TPA solution was added into the CdSe colloidal suspension. This mixture was then allowed to mix thoroughly in an ultrasonication bath. The temperature was kept at room temperature. The nanocrystals were precipitated using absolute ethanol and redispersed in toluene.

TAA and CTAA have limited solubility in toluene. Therefore, acetone and a very small amount of pyridine were added into toluene to aid the dissolution of the molecules. 100 mg of CdSe nanorods was dispersed in 7 mL of toluene. 617 mg (4 mmol) of TAA was dispersed in a mixture of 3 mL of acetone and 0.32 mL (4 mmol) of pyridine. The CdSe colloidal suspension and TAA solution were then mixed together in an ultrasonication bath at room temperature. For CTAA, 358 mg (2 mmol) of CTAA was dispersed in 3 mL of acetone and 0.16 mL (2 mmol) of pyridine. The CdSe colloidal suspension and TAA solution were then mixed together and ultrasonicated for 40 min at room temperature. The nanoparticles were then precipitated using absolute ethanol and redispersed in toluene. This step was repeated at least three times to ensure that the free ligands were washed away. CdSe nanorods that underwent a ligand-exchange process with TPA, TAA, and CTAA will be identified as CdSe–TPA, CdSe–TAA, and CdSe–CTAA, respectively in the following text. All of the nanoparticles were thoroughly dried in vacuum oven overnight to remove the excess solvent before they were used in solar-cell fabrication.

**Device Fabrication.** CdSe nanorods were dispersed in DCB unless otherwise stated, and P3HT was also dissolved in DCB separately. Both solutions were mixed together to form a mixture containing 90 wt % of CdSe. Indium tin oxide (ITO)-coated glass substrates (Kintec Co., 7 ohm/sq) were patterned using hydrochloric acid. The etched substrates were then cleaned in detergent, deionized water, acetone, and isopropanol sequentially for 15 min each in an ultrasonication bath. The substrates were cleaned by air plasma for 2 min. Air plasma cleaning was applied to remove organic substances on the surface of the substrate and to enhance the deposition of the PEDOT:PSS film afterward. A layer of PEDOT:PSS was spin-coated on plasma-cleaned ITO-coated glass substrates at 3000 rpm for 60 s and annealed at 140 °C for 10 min. Next, the photoactive layer was spin-coated from the blend solutions under a nitrogen environment. An aluminum cathode was deposited through a shadow mask by thermal evaporation at  $2 \times 10^{-6}$  mbar to form a device area of 7 mm<sup>2</sup>.

**Characterization.** The morphology of the CdSe nanorods was determined using transmission electron microscopy (TEM). TEM samples were prepared by drop-casting a few drops of the nanocrystals dispersion onto a lacey carbon-coated copper grid. In this study, the TEM studies were carried out using a JEOL 2010 TEM fitted with a LaB<sub>6</sub> filament operating at an acceleration voltage of 200 kV. The HSCs were tested in a nitrogen environment. The current density–voltage (*J*–*V*) characteristics of the devices were measured under 1 sun illumination (AM1.5G, 100 mW/cm<sup>2</sup>, simulated by Konica Minolta San-ei XES-301S solar simulator) using a Keithley SMU 2400 sourcemeter. External quantum efficiency (EQE) of the devices was

measured using a Newport Merlin radiometer, and a Hamamatsu calibrated silicon diode was used as the reference diode. The selection of the wavelength was carried out using a monochromator. The morphology of the film was determined using atomic force microscopy (AFM). The AFM images were obtained using a Digital Instrument Nanoscope IIIa. For femtosecond transient absorption spectroscopy (TAS) measurements, incident 650 nm, 150 fs pump pulses were generated from a Coherent TOPAS-C optical parametric amplifier that was pumped using a 1 kHz Coherent Legend regenerative amplifier, which was seeded by an 80 MHz Coherent Vitesse oscillator. Broadband probe pulses (450–800 nm) were generated by focusing a small portion (~5 μJ) of the fundamental 800 nm laser pulses into a 2 mm thick sapphire plate. The pump and probe pulses were cross-polarized to eliminate any contribution from coherent artifacts at early times. Pump-induced changes in transmission ( $\Delta T/T$ ) of the probe beam were monitored using a standard monochromator/PMT configuration with lock-in detection. The pump beam was chopped at 83 Hz, and this was used as the reference frequency for the lock-in amplifier.

## RESULTS AND DISCUSSION

CdSe nanorods used in these HSCs were synthesized using the hot coordinating solvent method, and the morphology of these nanoparticles is shown Figure 1a. These CdSe nanorods have a

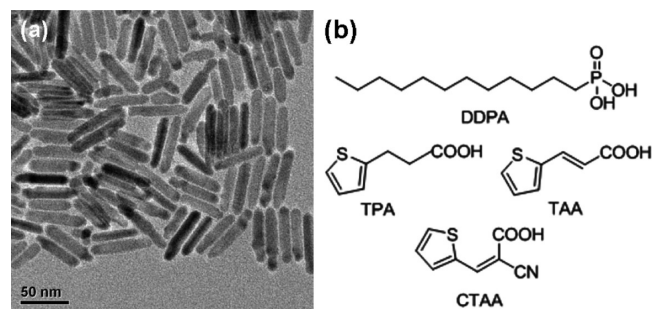


**Figure 1.** (a) TEM image of CdSe nanorods and (b) chemical structures of the original and replacing ligands used in this study.

diameter of approximately 10 nm and a length of 63 nm. The chemical structures of the original ligand, DDPA, and the replacing carboxylic acids ligands (with and without conjugated structure) are shown in Figure 1b. In TPA, the bridge between the thiophene group and carboxylic acid is unconjugated, whereas TAA and CTAA have conjugated bridges between both end groups.

The *J*–*V* characteristics of the P3HT:CdSe nanorods HSCs before and after ligand exchange are shown in Figure 2a, and the device characteristics of the HSCs are summarized in Table 1. All HSCs were measured in a glovebox under a nitrogen environment, and the measurements were corrected for spectral mismatch. It was observed that the HSCs fabricated using CdSe–DDPA nanorods exhibited a PCE of 0.69%, with short-circuit current density ( $J_{SC}$ ) of 2.37 mA/cm<sup>2</sup>, an open-circuit voltage ( $V_{OC}$ ) of 0.68 V, and a fill factor (FF) of 0.43. In general, the HSCs performance improved when ligand-exchanged CdSe nanorods were used. There is a slight improvement in the device performance for P3HT:CdSe–TPA HSCs. P3HT:CdSe–TPA HSCs have an average PCE of 0.76%. For P3HT:CdSe–TAA HSCs, the measured PCE increased to 1.30%, and for P3HT:CdSe–CTAA, a PCE of 1.12% was obtained. The improvement in the PCE comes from the increase in  $J_{SC}$  and FF, and this increase is very likely due to a reduction in donor–acceptor and interparticle distance after

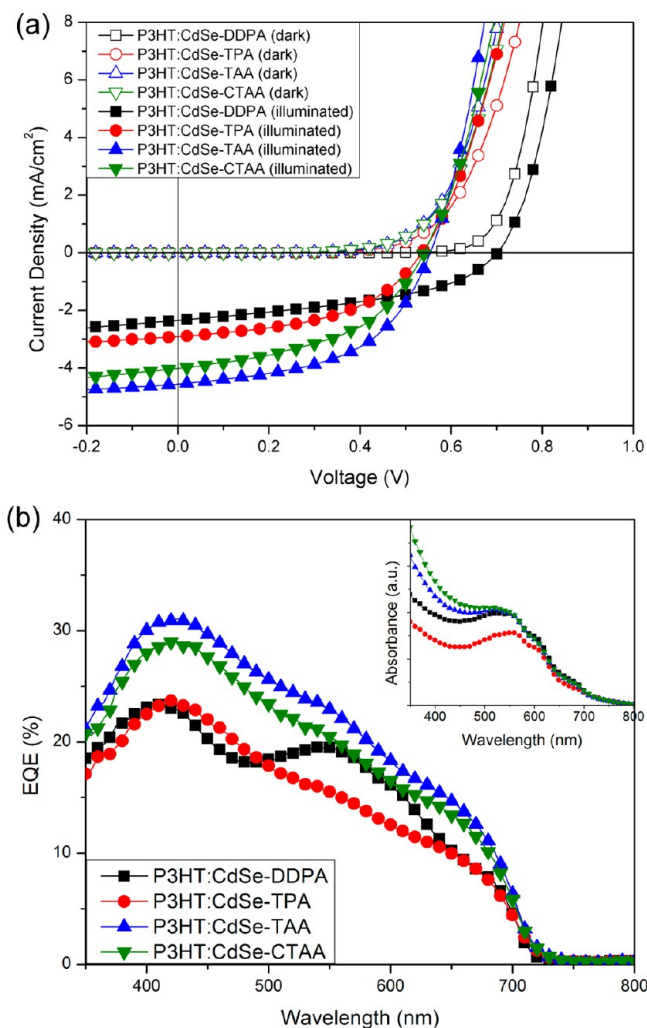


**Figure 2.** (a) Dark (open) and illuminated (solid)  $J$ - $V$  characteristics and (b) EQE spectra of P3HT:CdSe HSCs with different surface capping ligands: DDPA (square), TPA (circle), TAA (triangle), and CTAA (inverted triangle). The absorption profiles of the hybrid films are shown in the inset of panel b.

**Table 1. Summary of Photovoltaic Device Characteristics of P3HT:CdSe HSCs with Different Surface Capping Ligands**

ligands	PCE (%)	$J_{SC}$ (mA/cm <sup>2</sup> )	$V_{OC}$ (V)	FF
DDPA	0.69	-2.37	0.68	0.43
TPA	0.76	-2.90	0.54	0.48
TAA	1.30	-4.57	0.56	0.51
CTAA	1.12	-4.15	0.54	0.50

ligand exchange from DDPA to the shorter ligands, thus enhancing the charge transport. In P3HT:CdSe-TAA HSCs, the PCE and the  $J_{SC}$  were almost twice that of P3HT:CdSe-DDPA HSCs. It is observed that the PCE of the HSCs made with CdSe nanorods capped with either of the two conjugated ligands performed better than that of TPA.

All of the HSCs showed an EQE response up to 700 nm, as seen in Figure 2b. The inset in Figure 2b shows the absorption profiles of the four hybrid films with similar thickness to those used in the devices. The maximum EQE is very similar for P3HT:CdSe-TAA (31%) and P3HT:CdSe-CTAA HSCs (29%). The maximum EQE for P3HT:CdSe-TPA and P3HT:CdSe-DDPA HSCs is about 23%. All of the maxima

occur within a wavelength range of 400–450 nm. The lower EQE observed in the P3HT:CdSe-TPA HSCs can be attributed to the lower absorbance of the P3HT:CdSe-TPA film as compared to the TAA and CTAA samples. Because all of the blend solutions have the same CdSe loading of about 90 wt % and the donor and acceptor remain unchanged, this variation in absorption is most probably related to the dispersion issue of the CdSe-TPA nanorods. It is common for a hybrid film to have a rough surface morphology, and this tends to affect adversely the absorption of the film.<sup>29</sup> The dispersion of CdSe-TPA nanorods in P3HT was not as good as the dispersion of CdSe nanorods with TAA or CTAA. The CdSe nanorods started to aggregate even in the solution and resulted in an inhomogeneous distribution of CdSe aggregates in the film, thus adversely affected the absorption of the film. This inhomogeneous distribution can also be observed in the AFM images in Figure 3b. In general, all three hybrid films made of ligand-exchanged nanorods are morphologically rough as a result of the reduced colloidal stability of the CdSe nanorods after the ligand-exchange process. The P3HT:CdSe-TPA film is the roughest (root-mean-square (RMS) = 85 nm) among all the hybrid films fabricated using ligand-exchanged nanorods (the RMS of P3HT:CdSe-TAA is 51 nm and P3HT:CdSe-CTAA is 63 nm). This indicates that CdSe aggregates in P3HT:CdSe-TPA film is larger compared to the other two films. Larger aggregates will result in less donor-acceptor interfacial area for exciton dissociation. This could be one of the reasons for the lower performance observed in TPA samples. However, in the case of P3HT:CdSe-DDPA (Figure 3a), the thin film is smoother (RMS = 23 nm), which implied a more homogeneous mixture between the donor and acceptor phases, but these HSCs did not perform better than the ligand-exchanged samples. This may indicate that for these films the problem lies with charge collection/transport instead of the generation. The charge collection/transport between the nanorods in the P3HT:CdSe-DDPA films could be limited. Thus, to determine further the origin of this lower  $J_{SC}$  and FF, both the resistance of the cells and the charge-transfer dynamics in the thin films were studied.

$J_{SC}$  is expected to improve if the film morphology is relatively homogeneous and the interparticle conductivity is good. In general, the EQE spectra of the HSCs correlate well to the trend observed in  $J_{SC}$  presented in Table 1. The integrated  $J_{SC}$  values (from EQE data) of the ligand-exchanged samples are in good agreement with the measured  $J_{SC}$  (difference around 5%). In P3HT:CdSe-DDPA HSCs, the integrated  $J_{SC}$  was higher than the measured  $J_{SC}$ . This could be attributed to the limitation in charge transport at higher charge-carrier density.<sup>48</sup> From the absorption spectra in the inset, it can be observed that although the absorption is poorer for the films with CdSe-TPA nanorods, the EQE is seen to be comparable to that of CdSe-DDPA nanorods. EQE is a measure of absorption efficiency, exciton diffusion efficiency, exciton dissociation/charge-transfer efficiency, and charge-collection efficiency. Because the absorption for P3HT:CdSe-DDPA is better than the P3HT:CdSe-TPA films but the EQE is comparable to P3HT:CdSe-TPA samples and bulk heterojunction films, exciton diffusion efficiency is fairly high, which means that either the charge-transfer efficiency or the charge-collection efficiency must be better in the CdSe-TPA devices compared to the CdSe-DDPA ones. The EQE of devices fabricated using CdSe-TAA nanorods and CdSe-CTAA nanorods are very similar, although the CdSe-TAA sample has a slightly lower

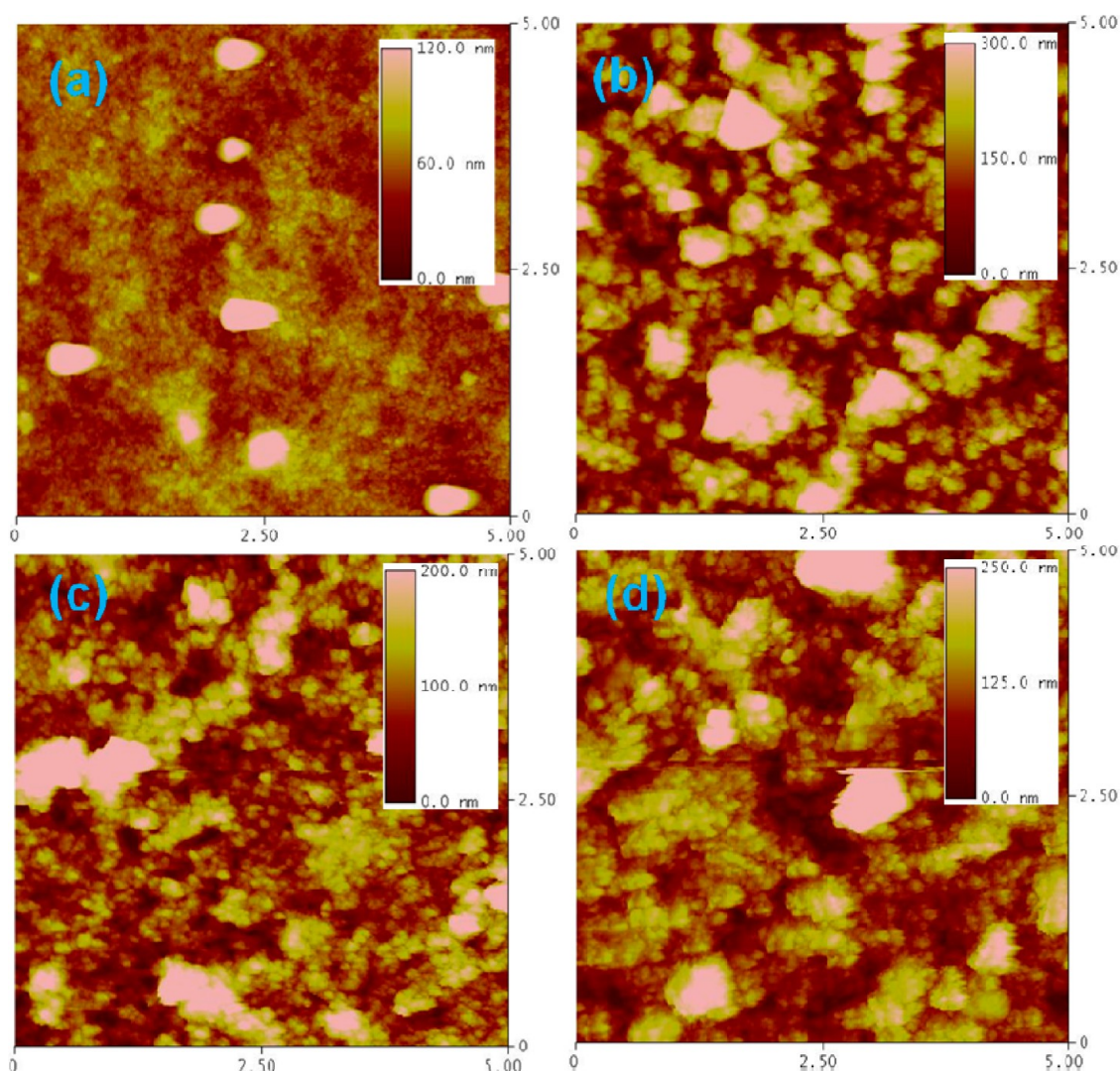


**Figure 3.** Tapping AFM images of (a) P3HT:CdSe-DDPA, (b) P3HT:CdSe-TPA, (c) P3HT:CdSe-TAA, and (d) P3HT:CdSe-CTAA hybrid films. The scan size is  $5 \times 5 \mu\text{m}^2$ .

**Table 2. Summary of Shunt and Series Resistance of P3HT:CdSe HSCs in the Dark and under Illumination**

hybrid devices (with different ligands)	dark		illuminated	
	$R_{\text{SHA}} (\Omega \text{ cm}^2)$	$R_{\text{SA}} (\Omega \text{ cm}^2)$	$R_{\text{SHA}} (\Omega \text{ cm}^2)$	$R_{\text{SA}} (\Omega \text{ cm}^2)$
P3HT:CdSe-DDPA	$1.3 \times 10^6$	3.8	$6.5 \times 10^2$	43.1
P3HT:CdSe-TPA	$1.4 \times 10^5$	7.9	$9.4 \times 10^2$	45.9
P3HT:CdSe-TAA	$7.1 \times 10^4$	5.1	$7.2 \times 10^2$	25.0
P3HT:CdSe-CTAA	$7.0 \times 10^4$	6.1	$8.0 \times 10^2$	30.7

absorption. The reason for this is due to the better film quality, which can be translated to lower series resistance (to be shown later). To understand how surface capping ligands are limiting the device performance, the electrical properties and also transient absorption properties of films were studied.

The shunt resistance ( $R_{\text{SHA}}$ ) and series resistance ( $R_{\text{SA}}$ ) of the HSCs can be determined from the slope of the  $J$ - $V$  characteristic at the applied voltage of 0 V and that at close to  $V_{\text{OC}}$  respectively, in the dark and under illumination.<sup>49,50</sup> The values are summarized in Table 2. Shunt resistance is usually a parasitic resistance that limits the leakage current. Leakage current is related to the presence of pinholes and leaky pathways in the active layer.<sup>51</sup> The large CdSe nanorods aggregates may act as possible pathways for the charges to flow

between electrodes and semiconductor and hence contributing to the leakage current and reducing the shunt resistance. Therefore, a large shunt resistance is more desirable for solar-cell applications. Despite the rougher surface morphology (Figure 3b), it is observed from Table 2 that P3HT:CdSe-TPA has a larger dark  $R_{\text{SHA}}$  ( $140 \text{ k}\Omega \text{ cm}^2$ ) compared to P3HT:CdSe-TAA and P3HT:CdSe-CTAA HSCs ( $70 \text{ k}\Omega \text{ cm}^2$ ). This seems to imply that the larger aggregates in the P3HT:CdSe-TPA film did not result in a lower shunt resistance. In fact, the shunt resistance in this film may be more related to the ease of interparticle charge transport. The non-conjugated structure in the TPA molecule may inhibit the interparticle charge transport and hence reduce the leakage current that flow through these CdSe aggregates. As a result, a

larger shunt resistance was observed in P3HT:CdSe-TPA HSCs. From the AFM images in Figure 3a, it is shown that P3HT:CdSe-DDPA film has the smoothest surface morphology. It was also observed in Table 2 that the  $R_{\text{SH}A}$  of P3HT:CdSe-DDPA is the highest ( $1300 \text{ k}\Omega \text{ cm}^2$ ) among the HSCs. This could possibly be explained with their thin-film morphology and the nature of the ligand. First, P3HT:CdSe-DDPA HSCs have less aggregates in the film. Therefore, the dark  $R_{\text{SH}A}$  is larger with less leaky pathways present in the hybrid film, which indicates a better thin-film quality. However, the bulky alkyl chain in the ligand is electrically insulating, which hinders the charge transport across the ligand, making the surface of the nanocrystals less conductive as compared to the ligand-exchanged nanorods. The  $R_{\text{S}A}$  of the HSCs in the dark are presented in Table 2. The dark  $R_{\text{S}A}$  values correlate well with the thin-film morphology of the HSCs. The smoothest P3HT:CdSe-DDPA film has a relatively smaller  $R_{\text{S}A}$  values than the other samples. The shunt and series resistance in the dark suggest that P3HT:CdSe-DDPA has a better thin-film quality for photovoltaic applications.

Under illumination, the  $R_{\text{SH}A}$  values of the HSCs were found to be considerably smaller than the  $R_{\text{SH}A}$  values in the dark. The smaller  $R_{\text{SH}A}$  under illumination originated from the substantially higher charge-carrier density in the photoactive layer when the HSCs are illuminated, which led to a higher leakage current at the electrode-semiconductor interfaces or charge recombination at defect states.<sup>52,53</sup> It was observed that the  $R_{\text{SH}A}$  of the HSCs under illumination were not significantly different from each other. This implies that they experienced similar situation with respect to charge dissociation and recombination at the donor-acceptor interfaces under illumination. The series resistances under illumination were determined from inverse of the slope at the  $V_{\text{OC}}$ . Generally the  $R_{\text{S}A}$  correlate to the bulk conductivity of the functional layer and the contact resistance between them.<sup>54</sup> It was observed that the P3HT:CdSe-DDPA and P3HT:CdSe-TPA HSCs had a higher  $R_{\text{S}A}$  among the HSCs. Their  $R_{\text{S}A}$  values were found to be at least 70% higher than P3HT:CdSe-TAA HSCs. This is an indication that the P3HT:CdSe-DDPA HSCs encounter higher resistance in the charge transport and collection at high charge-carrier density despite the better thin-film quality, as suggested by the higher dark  $R_{\text{SH}A}$ . This probably explains the difference in the EQE and  $J_{\text{SC}}$  of P3HT:CdSe-DDPA HSCs. From this discussion on the  $R_{\text{SH}A}$  and  $R_{\text{S}A}$  values of the HSCs, it is likely that the performance of these HSCs were not limited by the dissociation and recombination processes at the interfaces for different ligands; instead, there is a strong possibility that the charge transport across the nanocrystals is the limiting factor, as suggested by the  $R_{\text{SH}A}$  in the dark. It was suggested that the electron transport from one nanocrystal to another occurs via phonon-assisted hopping.<sup>55</sup> In addition, the electron-transport process depends largely on the spacing between the nanocrystals, which is governed by the size of the ligand.<sup>56</sup> To determine conclusively if this is the case, charge-transfer dynamics in these hybrid films were studied.

Photoinduced charge-transfer dynamics between P3HT and CdSe nanorods with different surface capping ligands were investigated with femtosecond TAS measurement. TAS is widely used for investigating the charge-carrier dynamics between heterostructures by monitoring the filling kinetics of the electron and hole states in the lowest-energy levels.<sup>39-41,43,57</sup> In this study, 650 nm (1.9 eV), 150 fs laser pulses were used to excite the electrons predominantly from

the CdSe nanorods (see Supporting Information, Figures S1 and S2). For pure CdSe nanorods capped with different ligands, a dominant photobleaching (PB) band (i.e.,  $\Delta T/T > 0$  over the 670–770 nm spectra range) was observed with a peak at 690 nm or 1.8 eV, as shown in Supporting Information, Figure S3. Such a PB signal in semiconductor nanostructures is dominated by the state filling of the 1S electron level, with a small contribution from the state filling of the 1S hole level.<sup>39-41,43,57</sup>

For P3HT:CdSe hybrid systems, the PB peak is slightly red-shifted as compared to that of pure nanorods. Such a red shift could arise from the variation in the dielectric constant of the surrounding medium. To extract the detailed charge-transfer and charge-carrier recombination times in the hybrid systems, the PB dynamics at the probe wavelength of 690 nm were monitored for both the pure and hybrid systems. Here, the pump fluence was kept to a minimal of  $0.25 \mu\text{J}/\text{cm}^2$  per pulse to mimic a low-intensity regime comparable to that for solar-cell operation to avoid any second-order effects. The decay curves and multiexponential fits of the systems are shown in Figures 4 and 5. Figure 4 clearly shows that an additional fast

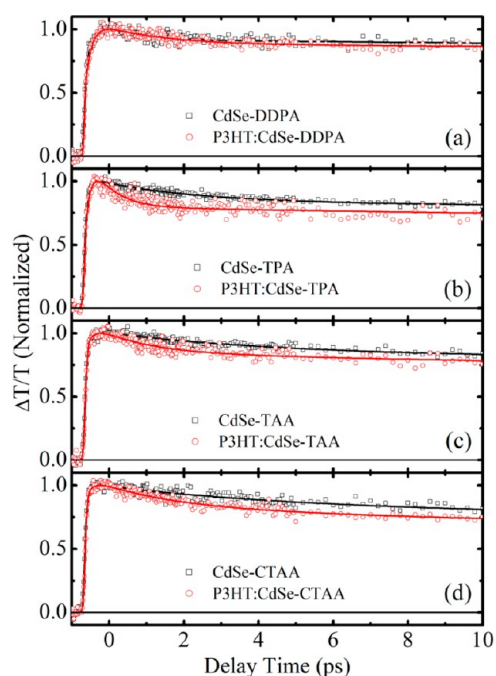


**Figure 4.** Normalized bleaching kinetics at 690 nm in the short time range show the additional rapid hole transfer from CdSe to P3HT in the P3HT:CdSe samples (circle) as compared to the CdSe nanorods samples (square) with different surface capping ligands following excitation at 650 nm (1 kHz, 150 fs,  $0.25 \mu\text{J}/\text{cm}^2$ ): (a) DDPA, (b) TPA, (c) TAA, and (d) CTAA.

decay process with small amplitude appears when the CdSe nanorods are blended with P3HT. Under the same experimental conditions, a negligible differential transmittance signal was observed in the pure P3HT film at 690 nm. Because of the higher position of the lowest unoccupied molecular orbital (LUMO) of P3HT (−3 eV) compared to the conduction band of CdSe (−4.5 eV), the electron transfer from the CdSe conduction band to the P3HT LUMO is not favored. Therefore, this additional fast decay could be assigned to the ultrafast valence band hole transfer from the CdSe valence band to the P3HT highest occupied molecular orbital (HOMO). The small amplitude is also consistent with the

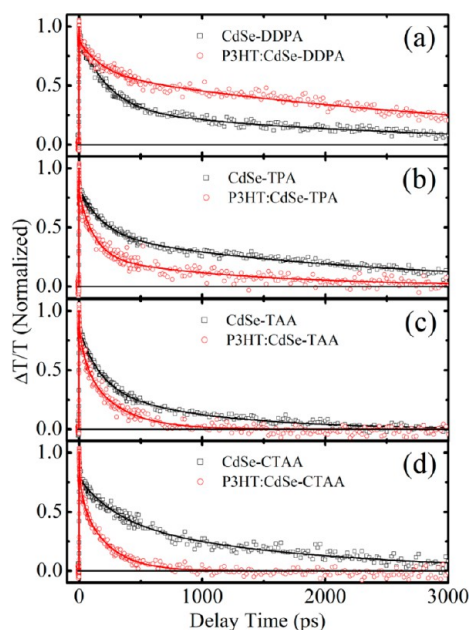


**Figure 5.** Normalized bleaching kinetics at 690 nm in the long time range show the charge-carrier recombination in CdSe nanorods samples (square) and in P3HT:CdSe samples (circle) with different surface capping ligands following excitation at 650 nm (1 kHz, 150 fs,  $0.25 \mu\text{J}/\text{cm}^2$ ): (a) DDDPA, (b) TPA, (c) TAA, and (d) CTAA.

small PB signal contributed by the hole filling in the lowest valence band. The hole-transfer lifetimes across different capping ligands were extracted and are listed in Table 3. It

**Table 3. Summary of Hole Transfer ( $\tau_{\text{HT}}$ ) and Charge Recombination ( $\tau_{\text{CR}}$ ) Lifetimes of P3HT:CdSe with Different Surface Capping Ligands**

ligand	$\tau_{\text{HT}}$ (ps)	$\tau_{\text{CR}}$ (ns)
DDPA	$7.0 \pm 0.7$	$3.3 \pm 0.3$
TPA	$1.3 \pm 0.2$	$1.1 \pm 0.1$
TAA	$2.6 \pm 0.3$	$0.27 \pm 0.03$
CTAA	$4.6 \pm 0.5$	$0.22 \pm 0.02$

clearly shows that the hole transfer from CdSe to P3HT is rapid (in the picoseconds range) for all of the capping ligands when the CdSe nanorods were excited. These transfer times are much faster than that for the charge recombination within the CdSe nanorods (in the nanoseconds range). The fast charge-carrier transfer between the energetically favored organic–inorganic nanostructure interface discussed here is consistent with recent TAS studies (i.e., hole transfer from hyperbranched CdSe nanocrystals to the hybrid P3HT is within 10 ps,<sup>42</sup> whereas the electron transfer from the CdSe quantum dots to the linked thiol-functionalized  $\text{C}_{60}$  could be as fast as 11 ps<sup>58</sup>).

The PB signal at 690 nm is dominated by state filling of the 1S electron level in the CdSe nanorods. Figure 5 shows the PB decays at this wavelength for all of the samples in the long time range. It clearly shows that the 1S electron dynamics in CdSe are significantly changed after the hybridization with P3HT. In pure CdSe nanorods, the PB dynamics at 690 nm represent the electron–hole recombination within the CdSe nanorods (which includes the contributions from the surface states and capping ligands). In P3HT:CdSe hybrid systems, the photo-excited holes are mainly located in P3HT. For the

recombination across the interfacial charge-transfer states, the electrons (in the CdSe conduction band) would have to tunnel out of the nanorods through the ligand shell to recombine with the holes (in the P3HT HOMO). The PB dynamics at 690 nm represent the 1S electrons recombination with the holes localized at the P3HT through tunneling. The intensity-weighted charge-carrier recombination times for P3HT:CdSe with different capping ligands are listed in Table 3. Among four capping ligands, DDDPA has the longest alkyl chain, which provides the highest barrier potential for the electrons to tunnel out of the nanorods core. This resulted in the slowest charge-carrier recombination between the CdSe nanorods and P3HT in the P3HT:CdSe–DDPA system. Figure 5 clearly shows that the 1S electron decays much slower in P3HT:CdSe–DDPA than in pure CdSe–DDPA nanorods and in other ligand-capped hybrid systems. The chemical structure of CTAA is similar to TAA except that there is an additional electron-withdrawing cyano group in CTAA molecules. However, the electron tunneling times through the TAA and CTAA ligands shell are very similar, as summarized in Table 3. This agrees well with the photovoltaic properties of the HSCs. This may indicate that the effect of the cyano group on the ligand was not prominent in this case. However, when the conjugated  $\text{C}=\text{C}$  bond in TAA is changed to a  $\text{C}-\text{C}$  bond (as in TPA), the electron-tunneling barrier will be raised, resulting in a longer electron-tunneling time, as shown in Figure 5. This again confirms our previous findings that the interparticle charge transport in P3HT:CdSe–DDPA and P3HT:CdSe–TPA HSCs is more difficult as compared to that in P3HT:CdSe–TAA HSCs.

From the evaluation of the resistances in the devices, it can be observed that the P3HT:CdSe–DDPA HSCs performed differently in the dark and in the light. The charge transport is believed to be poorer when in the light (i.e., high carrier density). These charges are likely to recombine eventually because of the difficulty in penetrating the insulating ligand shell. This issue was not as prominent in the HSCs fabricated using ligand-exchanged CdSe because of the more efficient charge transport across the ligand shell.

Therefore, from the above TAS studies, it can be clearly seen that the hole transfer from CdSe to P3HT in the hybrid systems can effectively compete with the interfacial charge-carrier recombination for all of the capping ligands. However, the electron tunneling from CdSe to the outside medium is strongly dependent on the capping ligand. Therefore, the device performance of these HSCs is most likely be limited by the electron transport between the nanorods. Our findings presented here are consistent with that from other publications (i.e., the main limiting factor in such type II nanocomposites is the charge-carrier trapping by the semiconductor nanocrystals, which hinders the efficient charge transport to the electrodes).<sup>42,58,59</sup>

## CONCLUSIONS

In this work, carboxylic acids-based molecules were studied as possible surface capping ligands because of their potential to control both the growth of the nanocrystals and the chemical and electrical properties of the interface between the nanocrystals and between the nanocrystals and polymer. It was found that the use of small conjugated ligands with a carboxylic group can improve the HSCs performance. It was observed that the HSCs made of ligand-exchanged CdSe nanorods performed better than that made of as-synthesized CdSe nanorods, mainly because of an improvement in the  $J_{\text{SC}}$  and FF. Both the thin-

film morphology and the shunt resistance in the dark indicate that P3HT: CdSe–DDPA hybrid films are more suitable for photovoltaic applications, but the HSCs performance was not better. The shunt resistances under illumination seemed to suggest that all HSCs encountered a similar situation at the donor–acceptor interfaces. Through the study of the surface morphology, the resistances of the cells, and the transient absorption spectra, it was found that these HSCs are limited by charge transport between the nanocrystals rather than the charge generation at the interface between the organic and inorganic phase. The charge injection from the nanocrystals to the polymer takes place in a very short time. In fact, the ideal system ought to have a more insulating interface between the organic and inorganic phase to suppress the recombination of the free charges but a more conducting pathway between the nanocrystals for efficient electron collection.

## ■ ASSOCIATED CONTENT

### Supporting Information

Linear absorption spectra of the capping ligands, P3HT, and CdSe nanorods, and the energy levels of P3HT and CdSe nanorods. This material is available free of charge via the Internet at <http://pubs.acs.org>.

## ■ AUTHOR INFORMATION

### Corresponding Authors

\*E-mail: [tzechien@ntu.edu.sg](mailto:tzechien@ntu.edu.sg) (T.C.S.).

\*E-mail: [ymlam@ntu.edu.sg](mailto:ymlam@ntu.edu.sg) (Y.M.L.).

### Author Contributions

#These authors contributed equally to this work.

### Notes

The authors declare no competing financial interest.

## ■ ACKNOWLEDGMENTS

This work is supported by a NTU start-up grant (M4080514), a SPMS Collaborative Research Award (M4080536), and the Competitive Research Programme under project no. NRF-CRP5-2009-04. G.X. and T.C.S. also acknowledge funding support from the Singapore NRF through the Singapore-Berkeley Research Initiative for Sustainable Energy (SinBeRISE) CREATE Programme. J.Y.L. also thanks Dr. Hairong Li for his contribution of materials and Dr. Teddy Salim and Kwan Hang Lam for useful discussions.

## ■ REFERENCES

- (1) Huynh, W. U.; Dittmer, J. J.; Alivisatos, A. P. *Science* **2002**, *295*, 2425–2427.
- (2) Huynh, W. U.; Dittmer, J. J.; Libby, W. C.; Whiting, G. L.; Alivisatos, A. P. *Adv. Funct. Mater.* **2003**, *13*, 73–79.
- (3) Dayal, S.; Kopidakis, N.; Olson, D. C.; Ginley, D. S.; Rumbles, G. *Nano Lett.* **2009**, *10*, 239–242.
- (4) Wang, L.; Liu, Y.; Jiang, X.; Qin, D.; Cao, Y. *J. Phys. Chem. C* **2007**, *111*, 9538–9542.
- (5) Lee, W.; Shin, S.; Han, S.-H.; Cho, B. W. *Appl. Phys. Lett.* **2008**, *92*, 193307-1–193307-3.
- (6) Kumar, S.; Nann, T. *J. Mater. Res.* **2004**, *19*, 1990–1994.
- (7) Gur, I.; Fromer, N. A.; Alivisatos, A. P. *J. Phys. Chem. B* **2006**, *110*, 25543–25546.
- (8) Cui, D.; Xu, J.; Zhu, T.; Paradee, G.; Ashok, S.; Gerhold, M. *Appl. Phys. Lett.* **2006**, *88*, 183111-1–183111-3.
- (9) Tan, Z.; Zhu, T.; Thein, M.; Gao, S.; Cheng, A.; Zhang, F.; Zhang, C.; Su, H.; Wang, J.; Henderson, R.; Hahm, J.-i.; Yang, Y.; Xu, J. *Appl. Phys. Lett.* **2009**, *95*, 063510-1–063510-3.
- (10) Watt, A. A. R.; Blake, D.; Warner, J. H.; Thomsen, E. A.; Tavenner, E. L.; Rubinsztein-Dunlop, H.; Meredith, P. J. *Phys. D: Appl. Phys.* **2005**, *38*, 2006.
- (11) Tsang, S. W.; Fu, H.; Wang, R.; Lu, J.; Yu, K.; Tao, Y. *Appl. Phys. Lett.* **2009**, *95*, 183505-1–183505-3.
- (12) Lin, Y.-Y.; Chu, T.-H.; Chen, C.-W.; Su, W.-F. *Appl. Phys. Lett.* **2008**, *92*, 053312-1–053312-3.
- (13) Lin, Y.-Y.; Chu, T.-H.; Li, S.-S.; Chuang, C.-H.; Chang, C.-H.; Su, W.-F.; Chang, C.-P.; Chu, M.-W.; Chen, C.-W. *J. Am. Chem. Soc.* **2009**, *131*, 3644–3649.
- (14) Beek, W. J. E.; Slooff, L. H.; Wienk, M. M.; Kroon, J. M.; Janssen, R. A. J. *Adv. Funct. Mater.* **2005**, *15*, 1703–1707.
- (15) Beek, W. J. E.; Wienk, M. M.; Janssen, R. A. J. *Adv. Mater.* **2004**, *16*, 1009–1013.
- (16) Greenham, N. C.; Peng, X.; Alivisatos, A. P. *Phys. Rev. B: Condens. Matter Mater. Phys.* **1996**, *54*, 17628–17637.
- (17) Kumar, S.; Nann, T. *Small* **2006**, *2*, 316–329.
- (18) Manna, L.; Scher, E. C.; Alivisatos, A. P. *J. Am. Chem. Soc.* **2000**, *122*, 12700–12706.
- (19) Peng, Z. A.; Peng, X. *J. Am. Chem. Soc.* **2002**, *124*, 3343–3353.
- (20) Xi, L.; Lam, Y. M. *Chem. Mater.* **2009**, *21*, 3710–3718.
- (21) Peng, X.; Manna, L.; Yang, W.; Wickham, J.; Scher, E.; Kadavanich, A.; Alivisatos, A. P. *Nature* **2000**, *404*, 59–61.
- (22) Jasieniak, J.; Bullen, C.; van Embden, J.; Mulvaney, P. *J. Phys. Chem. B* **2005**, *109*, 20665–20668.
- (23) Bullen, C. R.; Mulvaney, P. *Nano Lett.* **2004**, *4*, 2303–2307.
- (24) Talapin, D. V.; Rogach, A. L.; Mekis, I.; Haubold, S.; Kornowski, A.; Haase, M.; Weller, H. *Colloids Surf., A* **2002**, *202*, 145–154.
- (25) Kumari, K.; Kumar, U.; Sharma, S. N.; Chand, S.; Kakkar, R.; Vankar, V. D.; Kumar, V. *J. Phys. D: Appl. Phys.* **2008**, *41*, 235409.
- (26) Olson, J. D.; Gray, G. P.; Carter, S. A. *Sol. Energy Mater. Sol. Cells* **2009**, *93*, 519–523.
- (27) Sih, B. C.; Wolf, M. O. *J. Phys. Chem. C* **2007**, *111*, 17184–17192.
- (28) Radychev, N.; Lokteva, I.; Witt, F.; Kolny-Olesiak, J.; Borchert, H.; Parisi, J. r. *J. Phys. Chem. C* **2011**, *115*, 14111–14122.
- (29) Albero, J.; Martinez-Ferrero, E.; Iacopino, D.; Vidal-Ferran, A.; Palomares, E. *Phys. Chem. Chem. Phys.* **2010**, *12*, 13047–13051.
- (30) Aldakov, D.; Chandezon, F.; Bettignies, R. D.; Firon, M.; Reiss, P.; Pron, A. *Eur. Phys. J.: Appl. Phys.* **2006**, *36*, 261–265.
- (31) Owen, J. S.; Park, J.; Trudeau, P.-E.; Alivisatos, A. P. *J. Am. Chem. Soc.* **2008**, *130*, 12279–12281.
- (32) Lek, J. Y.; Xi, L.; Kardynal, B. E.; Wong, L. H.; Lam, Y. M. *ACS Appl. Mater. Interfaces* **2011**, *3*, 287–292.
- (33) Jeltsch, K. F.; Schädel, M.; Bonekamp, J.-B.; Niyamakom, P.; Rauscher, F.; Lademann, H. W. A.; Dumsch, I.; Allard, S.; Scherf, U.; Meerholz, K. *Adv. Funct. Mater.* **2012**, *22*, 397–404.
- (34) Said, A. J.; Poize, G.; Martini, C.; Ferry, D.; Marine, W.; Giorgio, S.; Fages, F.; Hocq, J.; Bouclé, J.; Nelson, J.; Durrant, J. R.; Ackermann, J. *J. Phys. Chem. C* **2010**, *114*, 11273–11278.
- (35) Jiang, X.; Chen, F.; Weiming, Q.; Yan, Q.; Nan, Y.; Xu, H.; Yang, L.; Chen, H. *Sol. Energy Mater. Sol. Cells* **2010**, *94*, 2223–2229.
- (36) Bouclé, J.; Chyla, S.; Shaffer, M. S. P.; Durrant, J. R.; Bradley, D. D. C.; Nelson, J. *Adv. Funct. Mater.* **2008**, *18*, 622–633.
- (37) Rempel, J. Y.; Trout, B. L.; Bawendi, M. G.; Jensen, K. F. *J. Phys. Chem. B* **2006**, *110*, 18007–18016.
- (38) Green, M. *J. Mater. Chem.* **2010**, *20*, 5797.
- (39) Klimov, V. I. *Annu. Rev. Phys. Chem.* **2007**, *58*, 635–673.
- (40) Robel, I.; Kuno, M.; Kamat, P. V. *J. Am. Chem. Soc.* **2007**, *129*, 4136–4137.
- (41) Xing, G.; Liao, Y.; Wu, X.; Chakraborty, S.; Liu, X.; Yeow, E. K. L.; Chan, Y.; Sum, T. C. *ACS Nano* **2012**, *6*, 10835–10844.
- (42) Grancini, G.; Biasiucci, M.; Mastria, R.; Scotognella, F.; Tassone, F.; Polli, D.; Gigli, G.; Lanzani, G. *J. Phys. Chem. Lett.* **2012**, *3*, 517–523.
- (43) Yang, Y.; Rodríguez-Córdoba, W.; Xiang, X.; Lian, T. *Nano Lett.* **2011**, *12*, 303–309.
- (44) Bansal, N.; Reynolds, L. X.; MacLachlan, A.; Lutz, T.; Ashraf, R. S.; Zhang, W.; Nielsen, C. B.; McCulloch, I.; Rebois, D. G.; Kirchartz,



T.; Hill, M. S.; Molloy, K. C.; Nelson, J.; Haque, S. A. *Sci. Rep.* **2013**, *3*, 1531-1–1531-8.

(45) Tagliazucchi, M.; Tice, D. B.; Sweeney, C. M.; Morris-Cohen, A. J.; Weiss, E. A. *ACS Nano* **2011**, *5*, 9907–9917.

(46) Morris-Cohen, A. J.; Peterson, M. D.; Frederick, M. T.; Kamm, J. M.; Weiss, E. A. *J. Phys. Chem. Lett.* **2012**, *3*, 2840–2844.

(47) Shi, D.; Cao, Y.; Pootrakulchote, N.; Yi, Z.; Xu, M.; Zakeeruddin, S. M.; Grätzel, M.; Wang, P. *J. Phys. Chem. C* **2008**, *112*, 17478–17485.

(48) Hardin, B. E.; Hoke, E. T.; Armstrong, P. B.; Yum, J.-H.; Comte, P.; Torres, T.; Frechet, J. M. J.; Nazeeruddin, M. K.; Gratzel, M.; McGehee, M. D. *Nat. Photon.* **2009**, *3*, 406–411.

(49) Moliton, A.; Nunzi, J.-M. *Polym. Int.* **2006**, *55*, 583–600.

(50) Xu, T.; Qiao, Q. *Energy Environ. Sci.* **2011**, *4*, 2700–2720.

(51) Ko, C.-J.; Lin, Y.-K.; Chen, F.-C.; Chu, C.-W. *Appl. Phys. Lett.* **2007**, *90*, 063509-1–063509-3.

(52) Nayar, P. S. *J. Appl. Phys.* **1982**, *53*, 1069–1075.

(53) Stubhan, T.; Oh, H.; Pinna, L.; Krantz, J.; Litzov, I.; Brabec, C. J. *Org. Electron.* **2011**, *12*, 1539–1543.

(54) Liu, J.; Wang, S.; Bian, Z.; Shan, M.; Huang, C. *Appl. Phys. Lett.* **2009**, *94*, 173107-1–173107-3.

(55) Chu, I.-H.; Radulaski, M.; Vukmirovic, N.; Cheng, H.-P.; Wang, L.-W. *J. Phys. Chem. C* **2011**, *115*, 21409–21415.

(56) Jarosz, M. V.; Porter, V. J.; Fisher, B. R.; Kastner, M. A.; Bawendi, M. G. *Phys. Rev. B: Condens. Matter* **2004**, *70*, 195327-1–195327-12.

(57) Zhu, H.; Song, N.; Lian, T. *J. Am. Chem. Soc.* **2010**, *132*, 15038–15045.

(58) Bang, J. H.; Kamat, P. V. *ACS Nano* **2011**, *5*, 9421–9427.

(59) Sharma, S. N.; Vats, T.; Dhenadhayalan, N.; Ramamurthy, P.; Narula, A. K. *Sol. Energy Mater. Sol. Cells* **2012**, *100*, 6–15.